How flat is the lower-mantle temperature gradient?

Marc Monnereau [a,*], David A. Yuen [b]

[a] *CNRS, Observatoire Midi-Pyrénées, 14 avenue Edouard Belin, 31400 Toulouse, France*
[b] *Minnesota Supercomputing Institute and Department of Geology and Geophysics, University of Minnesota, Minneapolis, MN 55455, USA*

Abstract

The temperature gradient in the lower mantle is fundamental in prescribing many transport properties, such as the viscosity, thermal conductivity and electrical conductivity. The adiabatic temperature gradient is commonly employed for estimating these transport properties in the lower mantle. We have carried out a series of high-resolution 3-D anelastic compressible convections in a spherical shell with the PREM seismic model as the background density and bulk modulus and the thermal expansivity decreasing with depth. Our purpose was to assess how close under realistic conditions the horizontally averaged thermal gradient would lie to the adiabatic gradient derived from the convection model. These models all have an endothermic phase change at 660 km depth with a Clapeyron slope of around -3 MPa K^{-1}, uniform internal heating and a viscosity increase of 30 across the phase transition. The global Rayleigh number for basal heating is around 2×10^6, while an internal heating Rayleigh number as high as 10^8 has been employed. The pattern of convection is generally partially layered with a jump of the geotherm across the phase change of at most 300 K. In all thermally equilibrated situations the geothermal gradients in the lower mantle are small, around 0.1 K km^{-1}, and are subadiabatic. Such a low gradient would produce a high peak in the lower-mantle viscosity, if the temperature is substituted into a recently proposed rheological law in the lower mantle. Although the endothermic phase transition may only cause partial layering in the present-day mantle, its presence can exert a profound influence on the state of adiabaticity over the entire mantle. © 2002 Elsevier Science B.V. All rights reserved.

Keywords: mantle; convection; geothermal gradient; spherical models; temperature

1. Introduction

The temperature gradient in the mantle is one of most important geophysical quantities because of its importance for estimating many of the transport properties, such as the viscosity [1,2], electrical conductivity [3,4] and thermal conductivity [5,6]. Because of the assumption of vigorous whole-mantle convection, the temperature gra-

dient in the lower mantle has usually be taken to be adiabatic for the purpose of constructing profiles of physical properties [7]. A value of 0.3 K km^{-1} [8–10] has been employed commonly by the geoscience community. Recently Yamazaki and Karato [2] have determined viscosity profiles in the lower mantle for realistic mantle flow laws based on diffusion experiments of silicon ion and melting point systematics. The value of the adiabatic temperature gradients assumed by Yamazaki and Karato [2] in order to obtain viscosity profiles which do not increase more than a factor of 30 across the lower mantle lies between 0.3 and 0.6 K km^{-1}.

* Corresponding author. Tel.: +33-561-332-968;
Fax: +33-561-332-900.
E-mail address: marc.monnereau@cnes.fr (M. Monnereau).

Recently Matyska and Yuen [11–13] using a 2-D cartesian model have examined the extent to which mantle temperature gradients deviate from the actual adiabatic profile on the basis of Bullen's parameter [14] as a criterion for adiabaticity. They found that there are regions in the mantle, such as the edges of plume heads or in the transition zone, where the temperature gradients can be substantially different from the adiabatic state.

The main purpose of this paper is to employ a realistic compressible 3-D spherical-shell model with different viscosity profiles and a background density and elastic stratification coming from the seismic preliminary reference Earth model (PREM) [15] together with an endothermic phase change to put tighter constraints on the temperature gradients in the lower mantle. Previous works on 3-D compressible spherical-shell convection [16–19] have not addressed this specific issue of the range of magnitude in the thermal gradient of the lower mantle under realistic conditions of delivering the current amount of surface heat flow. In this study we will focus our attention on this particular point by using realistic mantle parameter values in the 3-D spherical-shell calculations.

2. Description of the 3-D spherical model

This 3-D spherical model has been developed in the anelastic approximation (e.g. Jarvis and McKenzie [20]) and includes the thermodynamic effects due to a solid-state phase transition (e.g. Christensen and Yuen [21]). In this case the density depends on the temperature, the pressure and the mineral phases:

$$\rho = \rho_r \left(1 - \alpha(T - T_S) + \frac{p - p_h}{K_S} \right) + \delta\rho_{660} \Gamma(p_h, T) \tag{1}$$

where ρ_r is the reference adiabatic density profile, α the thermal expansion, T the temperature, T_S the adiabatic temperature, K_S the bulk modulus, p the pressure, p_h the hydrostatic pressure and $\delta\rho_{660}$ the density jump due to the endothermic spinel–post-spinel mineral phase transition. This phase

transition is prescribed by a sharply varying function depending on the temperature and the hydrostatic pressure:

$$\Gamma(p_h, T) = \frac{1}{2} \left[1 + \tanh\left(\frac{p_h - p_0 - \gamma T}{\delta p} \right) \right] \tag{2}$$

where γ and p_0 are respectively the Clapeyron slope and the pressure reference of the phase change and δp the half-width of the phase change. The anelastic approximation assumes that the density is only depth-dependent in the continuity equation:

$$\nabla \cdot (\rho_r \mathbf{u}) = 0 \tag{3}$$

where $\mathbf{u}$ is the velocity field. Because of the high viscosity of mantle rock, all inertial terms are neglected in the momentum balance, i.e. assuming an infinite Prandtl number:

$$\nabla \cdot \tau - \nabla p + \rho \boldsymbol{g} = \mathbf{0} \tag{4}$$

where τ is the deviatoric stress tensor and $\boldsymbol{g}$ the gravity. In the energy equation, the latent heat effects due to the dynamic pressure has been neglected, so that the energy conservation is given by:

$$\overline{C}_p \left[\rho_r \frac{\partial T}{\partial t} + \nabla \cdot (\rho_r \mathbf{u} T) \right] - \overline{\alpha} T \rho_r (\boldsymbol{g} \cdot \mathbf{u}) =$$

$$k \nabla \cdot (\nabla T) + \tau : (\nabla \mathbf{u}) + \rho_r \Phi \tag{5}$$

where k is the thermal conductivity, Φ the internal heating rate and $\overline{C}_p$ and $\overline{\alpha}$ are the heat capacity and the thermal expansivity altered by the latent heat effects and phase change:

$$\overline{C}_p = C_p + \frac{\gamma^2 T \delta\rho_{660}}{\rho_r^2} \frac{\partial \Gamma}{\partial p_h}$$
$$\overline{\alpha} = \alpha + \frac{\gamma \delta\rho_{660}}{\rho_r} \frac{\partial \Gamma}{\partial p_h} \tag{6}$$

For a depth-dependent viscosity in which the viscosity profile consists of various layers with different viscosity, the velocity field satisfying the continuity equation (Eq. 3) can be described by a

poloidal potential, Ψ:

$$\mathbf{u} = \frac{1}{\rho_{\mathrm{r}}} \nabla \times \nabla \times (\Psi \mathbf{e}^{\mathrm{r}}) \tag{7}$$

Expanding the poloidal function in spherical harmonics:

$$\Psi = \sum_{lm} \psi_{lm}(r) Y_{lm}(\theta, \varphi) \tag{8}$$

and introducing Eq. 7 into Eq. 4, the momentum balance yields the following fourth-order poloidal O.D.E. for each harmonic:

$$\dddot{\psi}_{lm} + \left(\frac{3\dot{\rho}_{\mathrm{r}}}{\rho_{\mathrm{r}}} - \frac{\rho_{\mathrm{r}}g}{K_{\mathrm{S}}} \right) \dddot{\psi}_{lm} +$$

$$\left(-\frac{3\ddot{\rho}_{\mathrm{r}}}{\rho_{\mathrm{r}}} + \frac{6\dot{\rho}_{\mathrm{r}}^2}{\rho_{\mathrm{r}}^2} - \frac{2l(l+1)}{r^2} - \frac{2\dot{\rho}_{\mathrm{r}}g}{K_{\mathrm{S}}} \right) \ddot{\psi}_{lm} +$$

$$\left(-\frac{\dddot{\rho}_{\mathrm{r}}}{\rho_{\mathrm{r}}} + \frac{6\ddot{\rho}_{\mathrm{r}}\dot{\rho}_{\mathrm{r}}}{\rho_{\mathrm{r}}^2} - \frac{6\dot{\rho}_{\mathrm{r}}^3}{\rho_{\mathrm{r}}^3} + \frac{3l(l+1)\dot{\rho}_{\mathrm{r}}}{r^2\rho_{\mathrm{r}}} + \frac{4l(l+1)}{r^3} + \right.$$

$$\left. \frac{\rho_{\mathrm{r}}g}{K_{\mathrm{S}}} \left(-\frac{\ddot{\rho}_{\mathrm{r}}}{\rho_{\mathrm{r}}} + \frac{2\dot{\rho}_{\mathrm{r}}^2}{\rho_{\mathrm{r}}^2} - \frac{l(l+1)}{r^2} \right) \right) \dot{\psi}_{lm} +$$

$$l(l+1) \left(\frac{\ddot{\rho}_{\mathrm{r}}}{r^2\rho_{\mathrm{r}}} - \frac{2\dot{\rho}_{\mathrm{r}}^2}{r^2\rho_{\mathrm{r}}^2} - \frac{4\dot{\rho}_{\mathrm{r}}}{r^3\rho_{\mathrm{r}}} + \frac{l(l+1)-6}{r^4} + \right.$$

$$\left. \frac{\rho_{\mathrm{r}}g}{K_{\mathrm{S}}} \left(-\frac{\dot{\rho}_{\mathrm{r}}}{3r^2\rho_{\mathrm{r}}} + \frac{2}{r^3} \right) \right) \psi_{lm} = -\frac{\rho_{\mathrm{r}}^2 g}{\eta} \overline{\alpha} \Theta_{lm} \tag{9}$$

where $\dot{\psi}$, $\ddot{\psi}$, ... and $\dot{\rho}$, $\ddot{\rho}$, ... denote respectively the first, second, ... radial derivative of ψ_{lm} and ρ_{r} (ψ_{lm} and ρ_{r} being only depth-dependent), Θ_{lm} being the spectral amplitude of the temperature field at degree l and order m. Note that the buoyancy term is the same one obtained in a 2-D approximation. For numerical purposes, we prefer this formulation which is equivalent to one in which all the mass heterogeneity induced by the phase change is located at the local depth where the phase change occurs. This approximation was previously adopted in a 3-D formulation [22].

Our spherical code is based on the approach for cartesian domain developed by Cserepes et al. [23] and was previously used in the Boussinesq ap-

proximation in Monnereau and Quere [24]. The energy equation is discretized by a finite-volume method [25], and solved by an alternating-direction-implicit scheme [26]. Then the resulting temperature field is expanded in spherical harmonics and the fourth-order poloidal O.D.E. (Eq. 9) is discretized by finite differences. In Eq. 9, the viscosity profile consists of several constant-viscosity layers, requiring four conditions at the interface between two different viscosity layers: the continuity of the radial velocity $\mathbf{u}^{\mathrm{r}}$, the continuity of the horizontal velocities $\mathbf{u}^{\theta\varphi}$ and the continuity of the normal and the tangential components of the radial stress tensor, $\boldsymbol{\tau}^{\mathrm{rr}} - p$ and $\boldsymbol{\tau}^{\mathrm{r}\theta\varphi}$ respectively. The top and the bottom boundaries are impermeable, stress-free and isothermal. Parameter values and the notations are listed in Table 1.

In the present study, the solutions have been integrated in time to more than the age of the Earth (10 Gy) for achieving statistical equilibrium on a coarse grid, $128 \times 64 \times 128$ points, corresponding to 128 regularly spaced radial levels and a maximum spherical harmonic degree $l = 64$. Then these solutions have been refined on a high-resolution grid, increasing the maximum spherical harmonic degree to $l = 256$ ($128 \times 256 \times 512$ points) for at least another 0.5 Gy.

3. Mantle properties and parameters

An estimate of the temperature gradient maintained dynamically in the mantle requires special care in the choice of the fluid properties and parameters used in the numerical simulations. The adiabatic gradient is mainly related to the thermal expansivity and the temperature by:

$$\left(\frac{\partial T}{\partial r} \right)_{\mathrm{s}} = -\frac{\alpha g T}{C_{\mathrm{p}}} \tag{10}$$

where the gravity, g, and the heat capacity, C_{p}, are assumed constant throughout the mantle. For this anelastic model, we have used the PREM model [15] as a reference state for the density and bulk modulus. ρ_{r} and K_{S} are exponential functions that fit PREM and that satisfy the fol-

lowing relationship:

$$\frac{\partial \rho_r}{\partial r} = \frac{\partial \rho_r}{\partial p_h} \frac{\partial p_h}{\partial r} = -\frac{\rho_r^2 g}{K_S} \qquad (11)$$

These are shown as the solid curves in Fig. 1. The thermal expansivity α is obtained by assuming a value of the Grüeneisen parameter of 1.0 and a classical limit for the specific heat at constant pressure C_p, using the specific values for the density and bulk modulus from the PREM model:

$$\alpha = \frac{\rho_r C_p}{K_S} \qquad (12)$$

The profile for α is shown as a light curve in Fig. 1. It decreases by about a factor of 4 across the mantle, a value consistent with the estimates for α, based on high-pressure experiments [27]. We note that many of the previous anelastic models [18,28,29] have employed analytical forms for the equation of state parameters instead of using the more realistic PREM model. We have kept the thermal conductivity, k, constant, unlike the depth-dependent thermal conductivity used by Balachandar et al. [28], Zhang and Yuen [18] and Tackley [29].

Other mantle properties and parameters affect the adiabatic gradient through the temperature. It is well known that the curvature of the top and bottom boundaries affects the symmetry of the boundary layers, inducing a global cooling of the convecting fluid. In the absence of depth-de-

Table 1
Notation and parameter values used

| Symbol	Meaning	Value	Unit (SI)
r, Θ, φ	spherical coordinates		m, rad, rad
r_{surf}	surface radius	6.371×10^6	m
r_{cmb}	CMB radius	3.491×10^6	m
d	mantle thickness	2.880×10^6	m
T	temperature		K
T_S	adiabatic temperature		K
T_{surf}	surface temperature	273	K
T_{cmb}	CMB temperature	3173	K
ΔT	temperature scale ($T_{cmb} - T_{surf}$)	2900	K
p	pressure		Pa
$\mathbf{u}$	velocity		m s^{-1}
$\mathbf{g}$	acceleration of gravity	10	m^2 s^{-2}
C_p	specific heat capacity at constant pressure	1200	J kg^{-1} K^{-1}
k	conductivity	3.3	W m^{-1} k^{-1}
α	thermal expansion profile		K^{-1}
α_0	thermal expansion at 660	1.94×10^{-5}	K^{-1}
K_S	bulk modulus profile		Pa
K_{S0}	bulk modulus at 660	269×10^9	Pa
η	viscosity		Pa s
η_{ref}	lower mantle viscosity	6×10^{22}	Pa s
ρ_r	density profile		kg m^{-3}
ρ_0	density at 660	4339	kg m^{-3}
Γ	phase function		
γ	Clapeyron slope	$-3 \times 10^6, -4 \times 10^6$	Pa K^{-1}
$\delta\rho$	density jump at 660	390	kg m^{-3}
δp	half-width of phase change	0.488×10^9	Pa
Φ	internal heating rate		W kg^{-3}
Q	whole internal heating	$30–60 \times 10^{12}$	W
ψ_{lm}	amplitude of the poloidal potential		
Θ_{lm}	amplitude of thermal heterogeneities		
l,m	degree and order		
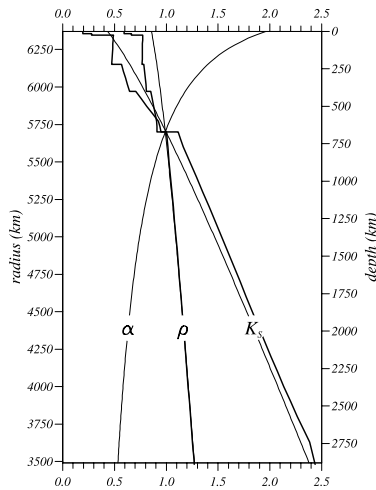
Fig. 1. Non-dimensional profiles of density, bulk modulus and thermal expansion used in the model (thin lines). The density and bulk profiles are exponential fit of PREM values [15], represented by thick lines. The extracted thermal expansion profile is based on the assumption that the Grüeneisen parameter and the heat capacity are constant. The dimensional values ρ_0, K_{S0} and α_0 used in the model, given in Table 1, correspond to the profiles at 660 km depth.

pendent properties and internal heating, the non-dimensional averaged temperature, which establishes at 0.5 in Cartesian geometry, decreases to 0.28 in the case of a geometry characteristic of the mantle [30]. This underscores the importance for our considering spherical geometry in the modelling.

Depth-dependent properties, such as viscosity increase with depth, introduce a similar effect [31]. In spite of the diversity of the viscosity profiles proposed, we have preferred to restrict our

study to a simple comparison of constant-viscosity cases with cases performed with a single stepwise increase in viscosity across the 660 km by a factor of 30, which is a classical viscosity profile used in models of mantle convection (e.g. Cserepes et al. [23]).

Lastly, the amount of internal heating is also a key parameter in the control of the mantle temperature. The mantle internal heating has two components: the radiogenic heating and the secular cooling. It is equal to the total heat released by the Earth, 44 TW [32], minus the heat supplied by radiogenic elements present in the crust and the heat delivered by the core, i.e. the basal heating. The average continental crust may contain 35–55% incompatible trace elements [33]. Since the chondritic composition of the Earth roughly corresponds to a radiogenic heating of 20 TW, the crustal part would be in the range of 7–11 TW, so that 33–37 TW are involved in the mantle dynamics. An estimation of the heat loss from the core is more problematic and subject to strong debate. The uncertainties come on the one hand from the core contents in radiogenic elements, and on the other from the growth rate of the inner core. It would be in the range of 2 TW to more than 10 TW [34]. As a result the mantle internal heating can be estimated to be between 23 TW and 35 TW, which corresponds to 70–95% of the heat involved in the mantle dynamics.

In most of our calculations, the internal heating has been set at 30 TW, but considering the uncertainty relative to this parameter some were performed in a wide range of values, from 0 to 60 TW. The reference viscosity has been chosen in

Table 2
Non-dimensional numbers

Symbol	Meaning	Expression	Value
Ra	Rayleigh number	$\dfrac{\rho_0^2 C_p g \alpha_0 \Delta T d^3}{\eta_{\mathrm{ref}} k}$	1.5×10^6
R	internal heating rate	$\dfrac{\rho_0 \Phi d^2}{k \Delta T}$	27–54
Rai	internal heating Rayleigh number	$\mathrm{Ra} \times R$	4–8×10^7
Di	dissipation number	$\dfrac{g \alpha_0 d}{C_p}$	0.48

order to obtained a high enough vigor convection to satisfy the total integrated power at the Earth's surface. The Rayleigh number (see Table 2 for expression) based on the higher viscosity is in the range of 10^6, leading to internal heating Rayleigh number values between 4.3×10^7 and 8.6×10^7. Table 3 lists the parameter values taken in the nine cases presented.

4. Results

We will now examine each of the physical effects on the adiabatic gradient maintained dynamically in 3-D compressible convection at a sufficiently high enough vigor.

In Fig. 2 we show a 3-D cross-section of the temperature fields taken from a representative case with some degree of layering present. Panels a and b represent models for depth-dependent thermal expansivity, $\alpha(r)$, and constant thermal expansivity respectively. They correspond to cases 1 and 2 in Table 3. Large plumes are observed to develop in the lower mantle in the case of variable α and they are able to breach the 660 km phase change. There is some partial layering caused by the ponding of the cold descending flow. For constant α, similar to the case of Machetel et al. [35], the plumes are poorly developed in the lower mantle and the style of layering is different from the variable α case. Thus we have shown that indeed variable α brings about a first-order effect in the style of 3-D spherical shell convection. This

phenomenon has already been found in earlier studies in 2-D cartesian convection [36,37].

Many of the background quantities in geodynamics, such as the temperature and density fields, are based on 1-D profiles, which have been horizontally averaged (i.e. they vary only with the radius). From our high-resolution 3-D calculations, we have extracted the 1-D profiles for the temperature, radial temperature gradient and the local adiabatic gradient and compare them for the cases listed in Table 3.

In Fig. 3 we display and compare the radial temperature profile (Fig. 3a) and the temperature gradient along with the adiabatic gradient (Fig. 3b) for three models, two with constant thermal expansivity, cases 2 and 3, and the other with depth-dependent thermal expansivity, case 1. The Rayleigh number for these systems based on the physical properties at 660 km is 1.6×10^6 for case 1, 3×10^6 for case 2 and 1×10^6 for case 3. There is a greater degree of layering for the lower Rayleigh number (case 3). This apparently contradicts the usual finding of other studies, a higher Rayleigh number meaning more layering. This variation in layering is more related to the different value of the thermal expansivity set in the three cases. The phase buoyancy parameter, $P = \gamma \delta \rho / \alpha_0 \rho_0^2 g d$ (e.g. Christensen and Yuen [21]), which expresses the phase change buoyancy to the thermal buoyancy ratio, depends strongly on the thermal expansivity. It is 0.111 for case 1, 0.072 for case 2 and 0.216 for case 3, so that a reduction by a factor of 3 of the thermal expansivity from

Table 3

| Case	Clapeyron slope (MPa K^{-1})	Thermal expansion (K^{-1})	Viscosity ratio low/up	Internal heating (TW)	R	Heat flux (TW) top	(TW) bottom	Viscous dissipation (TW)	T_{max} (K)
1	−3	PREM	30	30	27	40	10	7	3198
2	−3	3×10^{-5}	30	30	27	38.5	8.5	12	3192
3	−3	1×10^{-5}	30	30	27	38	8	3.8	3176
4	−3	PREM	1	30	27	34	4	5.5	3180
5	−4	PREM	1	30	27	35.5	5.5	5	3173
6	−4	PREM	30	30	27	41	11	7	3187
7	−3	PREM	30	0	0	12.5	12.5	3.3	3194
8	−3	PREM	30	15	13.5	25	12	6	3194
9	−3	PREM	30	60	54	67.5	7.5	11.4	3181
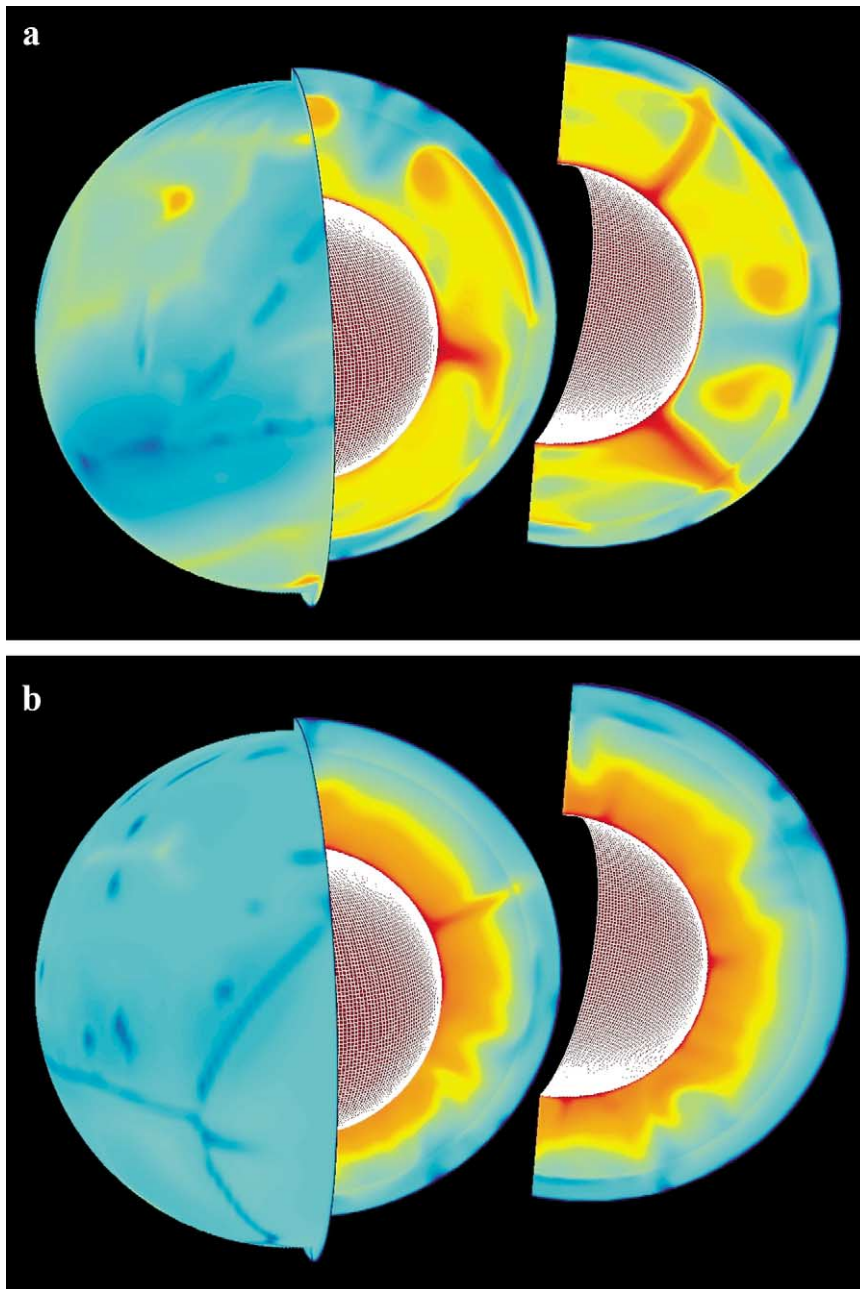
Fig. 2. Comparison between a case with depth-dependent thermal expansivity (case 1, panel a) and a case with constant thermal expansion (case 2, panel b). In both cases, there is a stepwise increase in the viscosity by a factor 30 from the upper to the lower mantle. The Rayleigh number based on the property values at 660 km depth and the higher viscosity is the same in both cases: 1.6×10^6.

case 2 to case 3 would be equivalent to a Clapey-ron slope three times steeper in case 3 than in case 2.

The thermal profile and also the gradient with variable α are lower than that with constant α, similar to the 2-D cartesian situations [37]. The temperature jumps across 660 km is not so large, about 300 K even in partially layered case. These jumps are much smaller than the assumed values in parameterized convection [38] and 3-D en-forced layered convection [39] of around 1000 K.

Next we compare in Fig. 3b the adiabatic tem-perature gradient, see Eq. 10 (solid curve): with the actual temperature gradient $\partial T/\partial r$ for the three cases. Substantial deviations between the adia-batic gradient and the temperature gradient are found in the upper mantle, especially in the vicin-
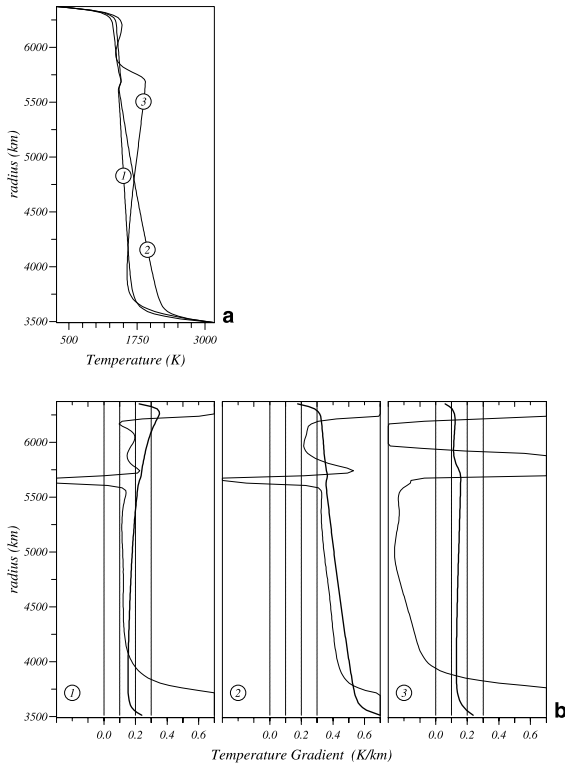
Fig. 3. Effect of the variable thermal expansivity. (a) Tem-perature profile of three different cases 1, 2 and 3. (b) Adia-batic gradient (thick curve) and the actual temperature gra-dient (thin curve). Case 1 uses depth-dependent thermal expansion, whereas cases 2 and 3 use constant values, 3×10^{-5} K^{-1} and 1×10^{-5} K^{-1} respectively (see Table 3 for details about the models).
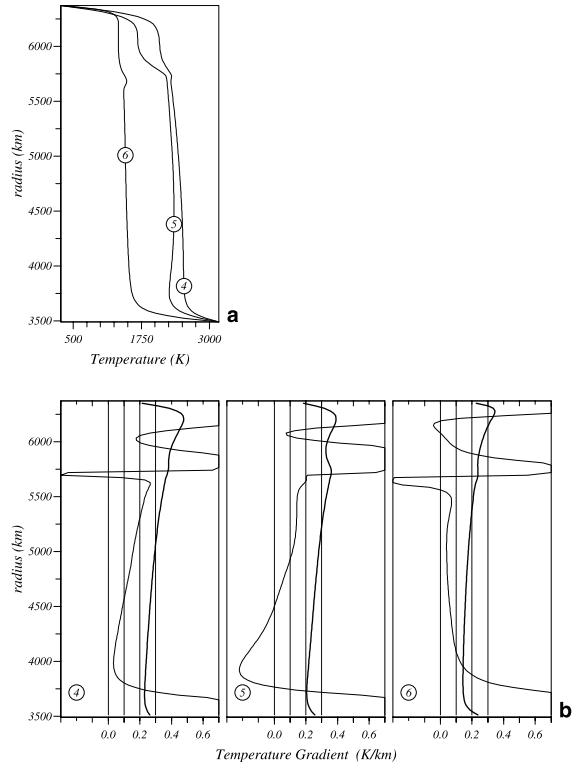

Fig. 4. Influence of the viscosity stratification. (a,b) The same as for Fig. 3 but for cases 4, 5 and 6. In cases 4 and 5, the viscosity is constant; it comprises a jump by a factor of 30 in case 6. The Clapeyron slope is -3 MPa K^{-1} in case 4 and -4 MPa K^{-1} in cases 5 and 6.

ity of the endothermic phase transition and the top boundary layer. In fact, the upper mantle on the average is not in an adiabatic state for all three cases. This same condition of non-adia-baticity has been found in the 2-D maps of non-adiabaticity due to deviations from Bullen's pa-rameter derived from the 2-D cartesian results of Matyska and Yuen [13]. In the lower mantle, the temperature gradient is slightly subadiabatic by less than 0.1 K km^{-1} for the two cases 1 and 2 in which whole-mantle circulation prevails, while for the partially layered case 3 the lower-mantle temperature gradient is strongly subadia-batic. We note that for constant α the thermal gradient in the lower mantle can be reduced by assuming low values of thermal expansivity, around 1×10^{-5} K^{-1}, as in the model of Machetel et al. [35].

The effects of viscosity stratification on 3-D spherical-shell convection have been investigated in the case of no phase transition by Zhang and Yuen [18,40] for both Boussinesq and compressible models respectively and by Bunge et al. [41] for the Boussinesq model. The influences of an endothermic phase transition with a depth-dependent viscosity in 3-D spherical-shell convection have been investigated by Bunge et al. [19]. However, the effects of compressibility, which include adiabatic and viscous heating, were not included in that particular model of Bunge et al. [19].

In Fig. 4, we compare the effects of having a viscosity jump across 660 km by a factor of 30, case 6 with two constant viscosity, cases 4 and 5, which have Clapeyron slopes of −3 MPa K^{-1} and −4 MPa K^{-1} respectively. The layering influence of decreasing the Clapeyron slope on mantle convection is well-known and is extremely sensitive to the magnitude of the Clapeyron slope between −3 and −4 MPa K^{-1} for viscosity profiles, which do not have a complex character, as a low-viscosity zone under 660 km [42]. However, we may note that the layering obtained with a constant viscosity and a strongly negative Clapeyron slope, case 5 disappears with the introduction of a stepwise viscosity increase with depth in case 6. Such a behavior was previously observed in axi-symmetric spherical simulations performed with exactly the same depth-dependent properties (ρ_r, α and K_S) [43]. On the other hand, the interior temperature for a viscously stiffer lower mantle (Fig. 4a) is much lower than those associated with constant viscosity and is well known from the early 2-D results of Gurnis and Davies [31].

In Fig. 4b, we show both the temperature gradient (light curve) and the adiabatic gradient (solid curve) for these three cases. Again the magnitude of the adiabatic gradients is not large and lies between 0.2 and 0.3 K km^{-1} in the lower mantle for the constant-viscosity cases 4 and 5. It is slightly lower by 0.1 K km^{-1} in case 6 which comprises a viscosity jump. Viscosity stratification does not exert a great influence on the magnitude of the adiabatic gradient throughout the mantle, as much as the magnitude and functional form of the thermal expansivity, shown above in Fig. 3. The lower mantle is subadiabatic in all cases, ex-
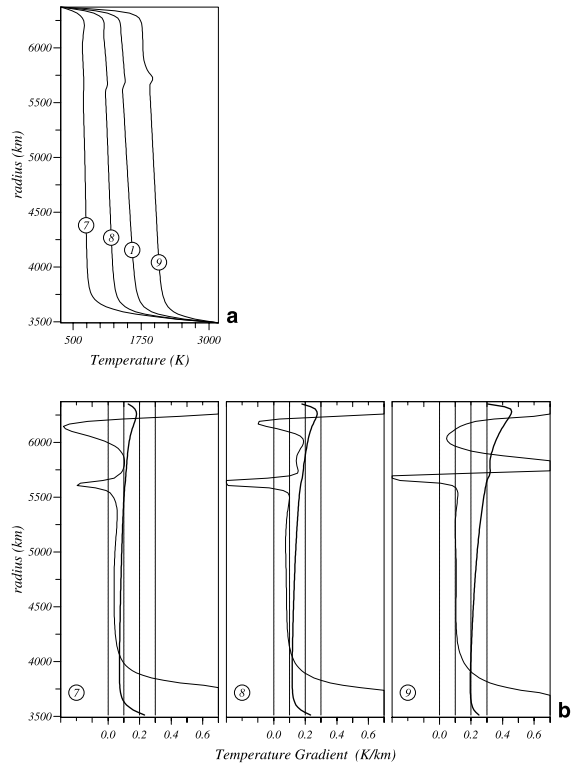

Fig. 5. Influence of the internal heating. (a,b) The same as for Fig. 3 but for cases 1, 7, 8 and 9. The non-dimensional internal heating is 0 in case 7, 13.5 in case 8, 27 in case 1 and 54 in case 9. In the four cases, the Clapeyron slope is −3 MPa K^{-1}, the properties are depth-dependent, and the viscosity is stratified.

cept a few hundred kilometers above the core–mantle boundary (CMB). In the upper mantle large departures from adiabaticity are found, again in agreement with the results based on Bullen's parameter by Matyska and Yuen [13] for temperature- and depth-dependent viscosity in cartesian 2-D models.

Internal heating can produce a noticeable increase in the averaged temperature of the mantle even in the presence of vigorous compressible convection [18,44]. In Fig. 5, we study the effects of increasing the internal heating from purely basal heating, case 7, to dimensional internal heating rate of 15 TW (case 8), 30 TW (case 1) and 60 TW (case 9). All four cases have both variable α and a viscosity jump of 30 from the upper to lower mantle. The combined effects from

variable α and a viscosity jump in the lower mantle (case 7) are to lower tremendously the interior temperature, but much more so to 1000 K in the lower mantle than in the case of 3-D cartesian compressible convection [28]. In the presence of these two depth-dependent properties of thermal expansivity and viscosity, even a very large amount of dimensional internal heating, 60 TW, which is around three times the chondritic heating value, cannot restore the mantle temperature back to a range of around 2500 K in the deep mantle. Some other mechanisms such as variable thermal conductivity [45] or greater degree of chemical layering in the deep mantle [46] are needed to bring the temperature back up higher. From Fig. 5b, we see that the magnitude of the adiabatic gradient is hardly changed by the amount of internal heating. They lie in the range of 0.1–0.25 K km^{-1}, with the larger value being associated with the largest amount of internal heating (case 9). This directly reflects the rise of the averaged temperature due to the augmentation of the internal heating rate (Fig. 5a). The temperature gradient in the lower mantle also progressively increases with the amount of internal heating, from 0.05 K km^{-1} to 0.1 K km^{-1}. In all cases, the lower mantle is maintained in a slightly sub-adiabatic state. This character is reinforced by the amount of internal heating, the difference being less than 0.05 K km^{-1} without internal heating in case 7 and reaching 0.15 K km^{-1} with the unrealistic value of 60 TW adopted in case 9. In spite of large uncertainties relative to the growth rate of the inner core, the percentage of internal heating involved in the Earth's mantle convection would fall in the range of 65% as in case 8 to 88% as in case 9, where the temperature gradient remains between 0.1 K km^{-1} and 0.15 K km^{-1} below the adiabatic gradient.

On the other hand, the upper mantle remains in a strongly non-adiabatic state because of the influence of the phase transition [13]. This feature has to be related to the proportion of upper mantle thickness affected by the thermal perturbation at 660 km and the top boundary layer, which may be a consequence of the absence of viscosity variation assumed in the models for the upper mantle. Nevertheless, note that the temperature gradient emphasizes the thickness of the thermal boundary layer roughly by a factor of two. This is particularly clear at the CMB. Therefore, it is not clear whether the presence of a low-viscosity channel below the lithosphere may bring back a large central part of the upper mantle close to the adiabatic state.

Our results on the adiabatic profiles show definitely that the common assumption of adiabaticity assumed in mantle convection may not be valid in the presence of phase transition. Furthermore, the adiabatic gradient would lie in the range of 0.1–0.25 K km^{-1}, clearly below the currently accepted value of 0.3 K km^{-1}, which is a direct consequence of the strong decrease with depth of the thermal expansivity. This is an important issue for petrology, since the potential temperature is commonly used for inference of mantle temperature from petrological samples. In Table 3 we also give other relevant thermomechanical quantities such as the total viscous heating, the maximum temperature attained in the flow and the amount of energy flowing across the top and bottom boundary layers. The total amount of viscous heating is not large and is only a fraction of the total amount of internal heating, but locally at plume heads or in stagnation points involving downwellings, the amount of viscous heating can surpass internal heating by a factor up to a 1000 in the case of temperature-dependent viscosity [47,48]. The maximum temperature T_{max} is around 10–20° higher than T_{cmb} and this excess temperature is smaller by a factor of 5 than those developed in variable-viscosity convection with shear heating [49]. We note that the T_{max} developed in the plume are steady-state values and in transient situations such as the plume being excited by a neighboring sinking cold current the maximum temperatures attained are much higher [50] and these local shear heating events may help to generate melts on the CMB [49].

5. Discussion and conclusions

Based on the above described sequence of results taken from 3-D spherical compressible con-

vection under sufficiently vigorous strength, we have found that it is very difficult to maintain an adiabatic temperature gradient in the Earth's lower mantle. Rather we found that all models produce a subadiabatic lower mantle with a superadiabatic portion in the bottom several hundred kilometers of the lower mantle. In all such cases, the state of adiabaticity in both the upper and lower mantle is strongly influenced by the presence of the endothermic phase transition at 660 km. A common feature of these models is that all models with internal heating can satisfy the global heat-flow constraint of delivering around 40 TW at the surface.

Within the spectrum of our convection models, we have encountered dynamical situations ranging from whole-mantle to partially layered convection. Partially layered, present-day mantle convection is also in accord with results obtained on the basis of direct seismic tomographic imaging of mantle circulation (e.g. Van der Hilst et al. [51]; Zhao [52]), which show that although some descending slabs penetrate into the lower mantle, others appear to be stopped in their descent at the depth of around 660 km depth [53].

In this range of realistic Rayleigh numbers our models reveal the great sensitivity of the system to the magnitude of the negative Clapeyron slope regarding the issue of being in a layered or partially layered state. Other distinct possibilities, such as the Clapeyron slope of the pyroxene-to-perovskite transition [54] or the potential existence of a regional low-viscosity zone under 660 km discontinuity [55,56], may have an impact on the sensitivity of the flow to the degree of layering. However, the degree of layering or the amount of internal heating do not alter too much the principal result of our findings that the temperature gradient in the lower mantle remains at around 0.05–0.15 K km^{-1}, a similar value attained also by the 2-D axi-symmetric calculations of Solheim and Peltier [57] and the 3-D results of Zhang and Yuen [18] and Bunge et al. [58]. These values are lower than the proverbial value of 0.3 K km^{-1} commonly employed in calculating the rheology of the lower mantle (e.g. Yamazaki and Karato [2]). Our robust finding of a relatively flat lower-mantle temperature gra-

dient of around 0.1 K km^{-1} would imply a much greater degree of viscosity stratification in the lower mantle than the predictions of Yamazaki and Karato [2] based on the commonly used value of 0.3 K km^{-1} and this low gradient value, 0.1 K km^{-1}, would then produce a high peak in the lower-mantle viscosity for the rheology used by Yamasaki and Karato [2] (S. Karato, personal communication), as inferred from the geoid studies by Ricard and Wuming [59] and Mitrovica and Forte [60]. Whether or not sufficient heat can be built up in this stagnant region must be determined from a high-resolution 3-D spherical-shell compressible convection calculation with variable viscosity.

Due to the endothermic phase change, which partially blocks the mantle circulation, the temperature gradient in the upper mantle does not lie on the adiabatic gradient at all and is very non-monotonic, especially in the case of layered convection. This situation can pose a serious problem for petrologists in the usage of potential temperatures in thermodynamic calculations. The temperature jumps across the 660 km is not so high, at most 300° for significantly layered convection. Previous estimates used for parameterized convection [38] were too large.

The lower-mantle geotherms in our models are all found to be subadiabatic. Therefore any sort of superadiabaticity inferred from seismology [61] or from mineral physics calculations [62] can only be explained by some sort of chemical stratification, which seems to be focussed more in the deep lower mantle [63–65]. The next step would be to make similar estimates for compressible thermal–chemical convection where the role of an enhanced radiogenic heating in the lower mantle [46] can be evaluated together with variable thermal conductivity [45], which raises the interior temperature and variable viscosity.

References

[1] S. Karato, Rheology of the lower mantle, Phys. Earth Planet. Inter. 24 (1981) 1–14.

[2] D. Yamasaki, S.-I. Karato, Some mineral physics constraint on the rheology and geothermal structure of Earth's lower mantle, Am. Mineral. 86 (2001) 385–391.

[3] X. Li, R. Jeanloz, Phases and electrical conductivity of a hydrous silicate assemblage at lower mantle conditions, Nature 350 (1991) 332–334.

[4] D.P. Dobson, J.P. Brodholt, The electrical conductivity and thermal profile of the Earth's mid-mantle, Geophys. Res. Lett. 27 (2000) 2325–2328.

[5] J.M. Brown, Interpretation of the D″ zone at the base of the mantle: depedence on assumed values of thermal conductivity, Geophys. Res. Lett. 13 (1986) 1509–1512.

[6] A.M. Hofmeister, Mantle values of thermal conductivity and the geotherm from phonon lifetimes, Science 283 (1999) 1699–1706.

[7] J.M. Brown, T.J. Shankland, Thermodynamic parameters in the Earth as determined from seismic profiles, Geophys. J. R. Astron. Soc. 66 (1981) 576–596.

[8] D.L. Turcotte, G. Schubert, Geodynamics: Applications of Continuum Physics to Geological Problems, Wiley, New York, 1982, 450 pp.

[9] F.D. Stacey, Physics of the Earth, 3rd edn., Brookfield Press, Brisbane, 1992.

[10] S. Spillopoulos, F.D. Stacey, The Earth's thermal profile: Is there a mid-mantle thermal boundary layer?, J. Geodyn. 1 (1984) 61–77.

[11] C. Matyska, D.A. Yuen, Profiles of Bullen parameter from mantle convection modelling, Earth Planet. Sci. Lett. 178 (2000) 39–46.

[12] C. Matyska, D.A. Yuen, Are mantle plumes adiabatic?, Earth Planet. Sci. Lett. 189 (2001) 165–176.

[13] C. Matyska, D.A. Yuen, Bullen's parameter η: A link between seismology and geodynamical modelling, Earth Planet, Sci. Lett. 198 (2002) 471–483.

[14] K.E. Bullen, An index of degree of chemical inhomogeneity in the Earth, Geophys. J. Int. 7 (1963) 584–592.

[15] A.M. Dziewonski, D.L. Anderson, Preliminary reference Earth model, Phys. Earth Planet. Inter. 25 (1981) 297–356.

[16] D. Bercovici, G. Schubert, G.A. Glatzmaier, Three-dimensional convection of an infinite Prandtl number compressible fluid in a basally heated spherical shell, J. Fluid Mech. 239 (1992) 683–719.

[17] P.J. Tackley, D.J. Stevenson, G.A. Glatzmaier, G. Schubert, Effects of multiple phase transitions in three-dimensional spherical model of convection in Earth's mantle, J. Geophys. Res. 99 (1994) 15877–15901.

[18] S. Zhang, D.A. Yuen, Various influences on plumes and dynamics in time-dependent, compressible mantle convection in 3-D spherical shell, Phys. Earth Planet. Inter. 94 (1996) 241–267.

[19] H.-P. Bunge, M.A. Richards, J.R. Baumgardner, A sensitivity study of three-dimensional spherical mantle convection at 108 Rayleigh number: Effect of depth-dependent viscosity, heating mode, and an endothermic phase change, J. Geophys. Res. 102 (1997) 11991–12007.

[20] G.T. Jarvis, D.P. McKenzie, Convection in compressible fluid with infinite Prandtl number, J. Fluid Mech. 96 (1980) 515–583.

[21] U.R. Christensen, D.A. Yuen, Layered convection induced by phase transitions, J. Geophys. Res. 90 (1985) 10291–10300.

[22] L. Cserepes, D.A. Yuen, On the possibility of a second kind of mantle plume, Earth Planet. Sci. Lett. 183 (2000) 61–71.

[23] L. Cserepes, M. Rabinowicz, C. Rosemberg-Borot, Three-dimensional infinite Prandtl number convection in one and two layers with implication for the Earth's gravity field, J. Geophys. Res. 93 (1988) 12009–12025.

[24] M. Monnereau, S. Quéré, Spherical shell models of mantle convection with tectonic plates, Earth Planet. Sci. Lett. 184 (2001) 575–587.

[25] S.V. Patankar, Numerical Heat Transfer and Fluid Flow, Hemisphere, New York, 1980.

[26] J. Douglas Jr., Alternating direction method for three space variables, Num. Math. 4 (1962) 41–63.

[27] A. Chopelas, R. Boehler, Thermal expansivity in the lower mantle, Geophys. Res. Lett. 19 (1992) 1983–1986.

[28] S. Balachandar, D.A. Yuen, D. Reuteler, Time-dependent three-dimensional compressible convection with depth-dependent properties, Geophys. Res. Lett. 19 (1992) 2247–2250.

[29] P.J. Tackley, On the ability of phase transitions and viscosity layering to induce long wavelength heterogeneity in the mantle, Geophys. Res. Lett. 23 (1996) 1985–1988.

[30] G.T. Jarvis, Curvature, heat flow and normal stresses in two-dimensional models of mantle convection, Phys. Earth Planet. Inter. 88 (1995) 17–29.

[31] M. Gurnis, G.F. Davies, Numerical study of high Rayleigh number convection in a medium with depth-dependent viscosity, Geophys. J. R. Astron. Soc. 85 (1986) 523–541.

[32] H.N. Pollack, S.J. Hurter, J.R. Johnson, Heat flow from the Earth's interior: analysis of the global data set, Rev. Geophys. 31 (1993) 267–280.

[33] R.L. Rudnick, D.M. Fountain, Nature and composition of the continental crust: a lower crustal perspective, Rev. Geophys. 33 (1995) 267–309.

[34] P.H. Roberts, C.A. Jones, A. Calderwood, Energy fluxes and Ohmic dissipation in the Earth's core, in: A.M. Soward, C.A. Jones, K.K. Zhang (Eds.), Earth's Core and Lower Mantle, Gordon and Breach, London, 2002 (in press).

[35] P. Machetel, C. Thoraval, D. Brunet, Spectral and geophysical consequences of 3-D spherical mantle convection with endothermic phase change at the 670 km discontinuity, Phys. Earth Planet. Inter. 88 (1995) 43–51.

[36] A.M. Leitch, D.A. Yuen, G. Sewell, Mantle convection with internal heating and pressure-dependent thermal expansivity, Earth Planet. Sci. Lett. 102 (1991) 213–232.

[37] U. Hansen, D.A. Yuen, S.E. Kroening, T.B. Larsen, Dynamical consequences of depth-dependent thermal expansivity and viscosity on mantle circulations and thermal structure, Phys. Earth Planet. Inter. 77 (1993) 205–223.

[38] T. Spohn, G. Schubert, Modes of mantle convection and the removal of heat from the earth's interior, J. Geophys. Res. 87 (1982) 4682–4696.

[39] G.A. Glatzmaier, G. Schubert, Three-dimensional spherical models of layered and whole mantle convection, J. Geophys. Res. 98 (1993) 21969–21976.

[40] S. Zhang, D.A. Yuen, The influences of lower mantle viscosity stratification on 3-D spherical shell mantle convection, Earth Planet. Sci. Lett. 132 (1995) 157–166.

[41] H.-P. Bunge, M.A. Richards, J.R. Baumgardner, Effect of depth-dependent viscosity on the planform of mantle convection, Nature 379 (1996) 436–438.

[42] L. Cserepes, D.A. Yuen, Dynamical consequences of midmantle viscosity stratification on mantle flows with an endothermic phase transition, Geophys. Res. Lett. 24 (1997) 181–184.

[43] M. Monnereau, M. Rabinowicz, Is the 670 km phase transition able to layer the Earth's convection in a mantle with depth-dependent viscosity?, Geophys. Res. Lett. 23 (1996) 1001–1004.

[44] P. Machetel, D.A. Yuen, Penetrative convective flows induced by internal heating and mantle compressibility, J. Geophys. Res. 94 (1989) 10609–10626.

[45] F. Dubuffet, D.A. Yuen, M. Rabinowicz, Effects of a realistic mantle thermal conductivity on the patterns of 3-D convection, Earth Planet. Sci. Lett. 171 (1999) 401–409.

[46] L.H. Kellogg, B.H. Hager, R.D. vanderHilst, Compositional stratification in the deep mantle, Science 283 (1999) 1881–1884.

[47] S. Balachandar, D.A. Yuen, D. Reuteler, G. Lauer, Viscous dissipation in three dimensional convection with temperature-dependent viscosity, Science 267 (1995) 1150–1153.

[48] P.F. Thompson, P.J. Tackley, Generation of mega-plumes from the core-mantle boundary in a compressible mantle with temperature-dependent viscosity, Geophys. Res. Lett. 25 (1998) 1999–2002.

[49] V. Steinbach, D.A. Yuen, Viscous heating: a potential mechanism for the formation of the ultralow velocity zone, Earth Planet. Sci. Lett. 172 (1999) 213–220.

[50] D.A. Yuen, O. Cadek, P. VanKeken, D.M. Reutler, H. Kyvalova, B.A. Schroeder, Combined results from mineral physics, tomography and mantle convection and their implications on global geodynamics, in: E. Boschi, G. Ekstrom, A. Morelli (Eds.), Seismic Modelling of Earth Structure, Editrice Compositri, Bologna, 1996, pp. 463–506.

[51] R.D. VanderHilst, S. Widiyantoro, E.R. Engdahl, Evidence for deep mantle circulation from global tomography, Nature 386 (1997) 578–584.

[52] D. Zhao, Seismic structure and origin of hotspots and mantle plume, Earth Planet. Sci. Lett. 192 (2001) 251–265.

[53] Y. Fukao, M. Obayashi, H. Inoue, N. Nenbai, Subducting slabs stagnant in the mantle transition zone, J. Geophys. Res. 97 (1992) 4809–4822.

[54] L. Chudinovskikh, R. Boehler, The $MgSiO_3$ ilmeniteperovskite phase boundary, EOS Trans. AGU, 82 Fall Meeting Suppl. (2001) F1136.

[55] M. Kido, O. Cadek, Inferences of viscosity from the oceanic geoid: Indication of a low viscosity zone below the 660-km discontinuity, Earth Planet. Sci. Lett. 151 (1997) 125–138.

[56] M. Kido, D.A. Yuen, The role played by a low viscosity zone under a 660 km discontinuity in the regional mantle layering, Earth Planet. Sci. Lett. 181 (2000) 573–583.

[57] L.P. Solheim, W.R. Peltier, Avalanche effects in phase transition modulated thermal convection: A model of the Earth's mantle, J. Geophys. Res. 99 (1994) 6997–7018.

[58] H.-P. Bunge, Y. Ricard, J. Matas, Non-adiabaticity in mantle convection, Geophys. Res. Lett. 28 (2001) 879–882.

[59] Y. Ricard, B. Wuming, Inferring the viscosity and the 3-D density structure of the mantle from geoid, topography and plate velocities, Geophys. J. Int. 105 (1991) 561–571.

[60] A.M. Forte, J.X. Mitrovica, Deep-mantle high-viscosity flow and thermomechanical structure inferred from seismic and geodynamic data, Nature 410 (2001) 1049–1056.

[61] B.L.N. Kennett, On the density distribution within the Earth, Geophys. J. Int. 132 (1998) 374–382.

[62] C.R.S. DaSilva, R.M. Wentzcovitch et al., The composition and geotherm of the lower mantle: constraints from the elasticity of silicate perovskite, Phys. Earth Planet. Inter. 118 (2000) 103–109.

[63] D.A. Yuen, U. Hansen, W. Zhao, A.P. Vincent, A.V. Malevsky, Hard turbulent thermal convection and thermal evolution of the mantle, J. Geophys. Res. 98 (1993) 5355–5373.

[64] M. Ishii, J. Tromp, Normal-mode and free-air gravity constraint on lateral variation in velocity and density of the Earth's mantle, Science 285 (1999) 1231–1236.

[65] S.I. Karato, B.B. Karki, Origin of lateral seismic wave velocities and density in the deep mantle, J. Geophys. Res. 106 (2001) 21771–21783.